Nanoscale Horizons

COMMUNICATION



Cite this: *Nanoscale Horiz.*, 2017, **2**, 277

Received 7th May 2017,
Accepted 15th June 2017

DOI: 10.1039/c7nh00066a

rsc.li/nanoscale-horizons

# Phosphorus-doped $NiCo_2S_4$ nanocrystals grown on electrospun carbon nanofibers as ultra-efficient electrocatalysts for the hydrogen evolution reaction†

Huahao Gu,[a] Wei Fan *[b] and Tianxi Liu *[ab]

**The development of highly efficient noble-metal-free electrocatalysts for the hydrogen evolution reaction (HER) is still a challenge nowadays. In this work, we prepared a highly active electrocatalyst containing phosphorus-doped $NiCo_2S_4$ nanocrystals grown on carbon nanotube embedded carbon nanofibers (P-$NiCo_2S_4$@CNT/CNF). The CNTs are involved in enhancing the electrical conductivity of the three-dimensional CNF network through a facile co-electrospinning method, which can facilitate electron transfer to the attached HER active material. Templated by this nanofiber network, the electroactive $NiCo_2S_4$ is confined to grow perpendicularly onto the CNT/CNF template *via* a hydrothermal reaction, thus exposing more catalytic active sites. Doping of P into the hybrid *via* a phosphidation reaction improves the electronic structure of the electroactive $NiCo_2S_4$, thus decreasing the energy barrier during the HER process. Owing to the synergistic effects from electrical enhancement and the nanostructured morphology, along with P-doping-induced optimization of the electronic structure, the P-$NiCo_2S_4$@CNT/CNF hybrid exhibits excellent HER performance, with an ultra-low onset overpotential ($\eta$) of 27 mV, a remarkable current density of 10 mA cm$^{-2}$ at $\eta$ as low as 74 mV, an impressive exchange current density of 0.79 mA cm$^{-2}$ and excellent long-term durability. Furthermore, its electroactivity exceeds that of most reported noble-metal-free electrocatalysts and is comparable to that of Pt, suggesting its great potential as a highly efficient HER catalyst.**

### Conceptual insights

Nickel cobalt sulfide ($NiCo_2S_4$), a ternary transition metal sulfide, has been largely reported as an electrode material in supercapacitors and lithium batteries. However, there is little detailed research on its application as an electrocatalyst for the hydrogen evolution reaction (HER). In this communication, $NiCo_2S_4$ is introduced as the HER active material grown on a template of carbon nanofibers, thus fully exposing its electrocatalytic sites. Despite its nanoscale structure, the hybrid exhibits an average performance in electrocatalysis. In this case, phosphorus (P) is delicately designed to dope into the electrocatalytically active $NiCo_2S_4$, which can modify the inherent electronic structure of catalysts, thus reducing the kinetic energy barrier in the HER process, and greatly enhancing its performance. Consequently, this communication not only broadens the application of $NiCo_2S_4$ in the energy field, but also provides an efficient method of doping to largely improve the HER activity of electrocatalyst.

## 1. Introduction

Hydrogen evolution through electrolysis of water provides a promising method to store energy from renewable sources.[1,2] Highly efficient electrocatalysts are required to promote the sluggish kinetics of the hydrogen evolution reaction (HER). Noble metals such as Pt are the state-of-the-art HER catalysts, but their scarcity and high cost limit their global-scale applicability. Recently, researchers have been developing high-performance earth-abundant metal chalcogenides, carbides, nitrides, or phosphides to replace Pt as electrocatalysts.[3–6] However, to the best of our knowledge, the existing reports mainly focus on researching some binary metal compounds, such as $CoS_2$, $MoSe_2$, $Mo_2C$ and $Ni_2P$, while only a few HER catalysts comprising ternary metal compounds have been reported. Nickel cobalt sulfide ($NiCo_2S_4$), a ternary transition metal sulfide, is intrinsically a conductive metal, which possesses an extremely high electrical conductivity[7] (~100 times as high as that of $NiCo_2O_4$, and much higher than those of the binary cobalt sulfides and nickel sulfides).[8,9] It has been reported that $Ni_xCo_{3-x}S_4$ polyhedra synthesized by transforming metal–organic frameworks through solvothermal sulfidation exhibit excellent HER activities, indicating the great potential of $NiCo_2S_4$ as an efficient electrocatalyst for hydrogen generation.[10]

In order to further improve the HER energy conversion efficiency, a general method is to hybridize the electroactive

[a] *State Key Laboratory of Molecular Engineering of Polymers, Department of Macromolecular Science, Fudan University, 220 Handan Road, Shanghai 200433, P. R. China. E-mail: txliu@fudan.edu.cn, txliu@dhu.edu.cn; Fax: +86-21-65640293; Tel: +86-21-55664197*

[b] *State Key Laboratory for Modification of Chemical Fibers and Polymer Materials, College of Materials Science and Engineering, Donghua University, 2999 North Renmin Road, Shanghai 201620, P. R. China. E-mail: weifan@dhu.edu.cn*

† Electronic supplementary information (ESI) available. See DOI: 10.1039/c7nh00066a

material with a highly conductive template to make a hybrid product. It is well known that the catalytic activity of an electrocatalyst is greatly influenced by the density of active sites. Hence, by introducing a conductive template with a large surface area, the electroactive material is confined to grow into a nanoscale structure, thus maximizing the exposure of HER active sites, as well as guaranteeing the fast electron transport in the hybrid. Carbon nanofiber (CNF) membranes with a three-dimensional (3D) network structure, high surface-to-volume ratio, and good conductivity have been commonly used as conductive templates in electrochemical energy storage and conversion devices.[11] Electrospinning techniques offer a versatile way to construct 3D CNF networks and their hybrids with tunable structures.[12,13] The performance of the electrospun nanofibers can be easily adjusted by changing the components of the spinning solution. For example, $NiCo_2O_4$-doped CNF membranes can be formed through co-electrospinning of polyacrylonitrile (PAN) and nickel–cobalt layered double hydroxide (Ni–Co LDH), followed by carbonization.[14] The uniformly distributed $NiCo_2O_4$ nanoparticles in CNF increase the conductivity of CNF and enhance the pseudocapacitive performance for supercapacitor applications.

Apart from constructing hierarchical hybrids of confined electroactive material with a highly conductive template, doping of non-metal heteroatoms into electrocatalysts is an effective approach to intrinsically improve the HER activity. The enhanced HER activities are contributed by the improved charge transfer between the foreign atom and the host atom, along with the modified inherent electronic structure reducing the kinetic energy barrier during the hydrogen generation pathway.[15] Gong *et al.* prepared ultrathin $MoS_{2(1-x)}Se_{2x}$ alloy nanoflakes with monolayered or few-layered thickness, which exhibited enhanced electrocatalytic performance in comparison with either $MoS_2$ or $MoSe_2$. The improvements resulted from the higher intrinsic activity of doped catalysts with tuned hydrogen adsorption free energy ($\Delta G_H$) closer to thermoneutral.[16] A similar result has also been reported for $WS_{2(1-x)}Se_{2x}$ nanotubes.[17] Despite doping or alloying with non-metal elements from the same group, more remarkable adjustment of electronic structure is expected to occur in the case of doping with non-metal heteroatoms from different groups, such as doping selenium to phosphor, and chlorine to sulfur. For example, a selenium-doped pyrite-phase $NiP_2$ nanostructure was designed for HER catalysis, and a current density of 10 mA $cm^{-2}$ was achieved at an overpotential as low as 84 mV, which was far smaller than that of pure $NiP_2$ (135 mV), highlighting the significant effect induced from doping or alloying electrocatalysts with non-metal element from another group.[18]

Herein, P-doped $NiCo_2S_4$ grown on carbon nanotube reinforced carbon nanofibers (P-$NiCo_2S_4$@CNT/CNF) has been prepared as a hybrid catalyst for the HER. CNTs are embedded into the CNF membrane *via* a facile co-electrospinning process, which is designed to increase the electrical conductivity of the template, facilitating the charge transfer between the CNT/CNF template and electroactive $NiCo_2S_4$ nanocrystals. P, a non-chalcogen heteroatom, is doped into $NiCo_2S_4$ to tune the electronic structure, thus optimizing the hydrogen adsorption energy of the hybrid catalyst. As a consequence, the P-$NiCo_2S_4$@CNT/CNF hybrid exhibits superb HER activity, with a large cathodic current of 10 mA $cm^{-2}$ at a low overpotential of 74 mV, an impressive exchange current density of 0.79 mA $cm^{-2}$, suggesting the rational design of the electrocatalyst.

# 2. Experimental

## 2.1. Preparation of P-$NiCo_2S_4$@CNT/CNF membranes

CNT/CNF membranes were prepared *via* facile co-electrospinning of polyacrylonitrile (PAN) and CNT dispersions, followed by pre-oxidation and carbonization (see the ESI† for experimental details). $NiCo_2S_4$@CNT/CNF membranes were prepared through a one-step hydrothermal procedure. Briefly, $Ni(NO_3)_2{\cdot}6H_2O$ (1 mmol), $Co(NO_3)_2{\cdot}6H_2O$ (2 mmol), thiourea (8 mmol) and urea (4 mmol) were dissolved in 30 mL DI water under vigorous magnetic stirring for 20 min. After that, the transparent pink solution was transferred into a 50 mL Teflon-lined stainless steel autoclave with a piece of CNT/CNF membrane ($2 \times 2$ $cm^2$) immersed into the reaction solution and maintained at 160 °C for 12 h.

P-doped $NiCo_2S_4$@CNT/CNF membranes were synthesized through a phosphidation reaction in a tube furnace. The phosphidation reaction was performed at 300 °C for 1 h with a heating rate of 2 °C $min^{-1}$ under a steady flow of $N_2$ gas. After cooling down naturally, the phosphorus-doped hybrid product was prepared, and denoted as P-$NiCo_2S_4$@CNT/CNF. The whole preparation process is schematically shown in Scheme 1. For comparison, a $NiCo_2S_4$@CNT/CNF hybrid was synthesized by the same process in the absence of phosphidation reaction while a P-$NiCo_2S_4$@CNF hybrid was synthesized without the addition of CNTs during the electrospinning step. Pure $NiCo_2S_4$ was prepared by a similar process without the CNT/CNF template and the phosphidation reaction.

## 2.2. Electrochemical measurements

The electrochemical measurements were carried out in a three-electrode setup using a CHI 660D electrochemical workstation (Shanghai Chenhua Instrument Co., China), with a graphite rod used as the counter electrode, a saturated calomel electrode (SCE) as the reference electrode, and the electrocatalyst modified glassy carbon electrode (GCE) as the working electrode. A piece of pre-cut hybrid membrane was affixed onto a GCE tip by Nafion solution, with a loading amount of 0.7–0.9 mg in a $3 \times 3$ $mm^2$ sized square shape. Commercial platinum wire (Pt) was also measured to establish a reference point of a state-of-the-art HER catalyst. Linear sweep voltammetry (LSV) was measured at a scan rate of 2 mV $s^{-1}$ in 0.5 M $H_2SO_4$ solution. All of the potentials were calibrated to the reversible hydrogen electrode (RHE) by adding a value of (0.241 + 0.059 × pH) V. The polarization curves were replotted as overpotential ($\eta$) *versus* log current density ($\log j$) to get the Tafel plots for assessing the HER kinetics. By fitting the linear portions of Tafel plots to the Tafel equation ($\eta = b\log(j) + a$), the Tafel slope ($b$) can be calculated. To determine the double-layer capacitance ($C_{dl}$) of electrocatalysts, cyclic voltammogram cycles were recorded in the region of 0.15–0.25 V *vs.* RHE at various scan rates. By

 

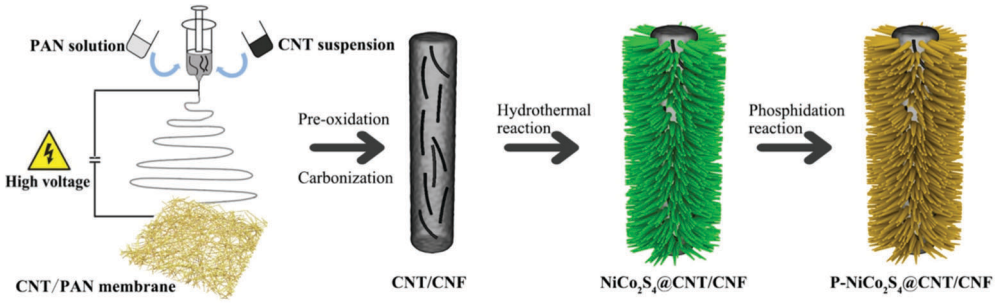


Scheme 1 Schematic illustration of the preparation of the P-$NiCo_2S_4$@CNT/CNF hybrid.

plotting the $\Delta j$ at 0.2 V *vs.* RHE against each scan rate, these data could be fitted to a line, whose slope is twice the geometric $C_{dl}$. Electrochemical impedance spectroscopy (EIS) measurement was performed in the same configuration under various overpotentials in frequencies ranging from $10^6$ Hz to $10^{-2}$ Hz with an amplitude of 5 mV. The electrocatalytic stability of the catalyst was evaluated by testing current–time responses under a fixed overpotential for a period of time.

## 3. Results and discussion

### 3.1. Morphology and structure of the P-$NiCo_2S_4$@CNT/CNF hybrid

A CNT-embedded CNF membrane was fabricated through co-electrospinning, pre-oxidation, and carbonization processes. As shown in Fig. 1, the surface of CNT/CNF becomes coarse due to the incorporation of CNTs. Some CNTs are partially exposed on the surface of the CNF while major parts are embedded into the nanofibers, which can be proved by the TEM observations (Fig. 1D). Moreover, the electrical conductivity of the CNT/CNF membrane is 1.90 S $cm^{-1}$, which is nearly three times that of the pure CNF membrane (Table S1, ESI†), thus promoting the charge transfer between the conductive template and electroactive $NiCo_2S_4$ during the HER process.

Based on the CNT/CNF template, P-$NiCo_2S_4$@CNT/CNF hybrids were prepared through a one-step hydrothermal method, followed by the phosphidation reaction. Fig. 2 shows the morphology of the $NiCo_2S_4$@CNT/CNF hybrid and P-$NiCo_2S_4$@CNT/CNF hybrid. It can be observed that $NiCo_2S_4$ nanocrystals with lengths around 200 nm are uniformly and densely grown onto the CNT/CNF template (Fig. 2A and B), whose morphology is the same as that of the $NiCo_2S_4$@CNF hybrid in general (Fig. S1, ESI†). For comparison, $NiCo_2S_4$ prepared in the absence of CNT/CNF membranes forms agglomerates with inhomogeneous nanorod and nanoflake interlaced morphology (Fig. S2, ESI†). Therefore, constructing hierarchical nanostructures of $NiCo_2S_4$ nanocrystals perpendicularly grown onto CNT/CNF can greatly prevent the aggregation of $NiCo_2S_4$, effectively exposing the electrocatalytic sites. After the phosphidation reaction, the overall morphology of the obtained P-$NiCo_2S_4$@CNT/CNF hybrid remains almost the same as that of $NiCo_2S_4$@CNT/CNF (Fig. 2C and D). However, EDS mapping clearly reveals the existence of P element in the P-$NiCo_2S_4$@CNT/CNF hybrid in addition to Ni, Co, C, and S elements (Fig. 2H). Compared with the EDS spectra of $NiCo_2S_4$@CNT/CNF (Fig. 2J and Fig. S3F, ESI†), an additional peak located at 2.01 keV can be found for the P-$NiCo_2S_4$@CNT/CNF hybrid, which refers to p$K_a$ energy, confirming the successful doping of P element *via* phosphidation reaction.[19]

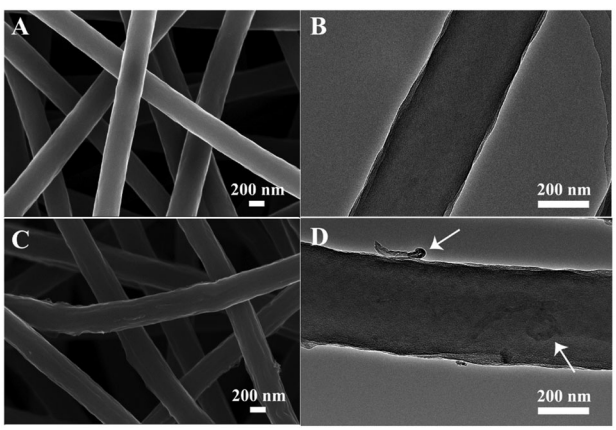


Fig. 1 FESEM (left) and TEM (right) images of (A and B) pristine CNF, and (C and D) CNT/CNF.

The phase purity of the as-prepared products has been investigated by XRD analysis (Fig. 3A). The CNT/CNF membrane shows a broad and weak peak at $2\theta = 26^\circ$, implying its amorphous structure. The XRD pattern of the $NiCo_2S_4$@CNT/CNF hybrid displays diffraction peaks at $2\theta$ = 16.7°, 27.2°, 31.9°, 38.6°, 50.8° and 55.6°, which can be, respectively, attributed to the (111), (220), (311), (400), (511), and (440) planes of $NiCo_2S_4$ (JCPDS 20-0782).[20,21] The XRD pattern of the P-$NiCo_2S_4$@CNT/CNF hybrid is consistent with that of the $NiCo_2S_4$@CNT/CNF hybrid, illustrating that the incorporation of P element does not cause changes in the XRD pattern of the hybrid, and a similar phenomenon has been reported previously.[22] In addition, for the synthesized $NiCo_2S_4$ agglomerates in the absence of CNT/CNF template, although its main diffraction peaks can be attributed to the planes of $NiCo_2S_4$, there appear several small extra peaks with impurities, suggesting that the attached $NiCo_2S_4$ nanocrystals can grow in higher purity with the support of the 3D CNT/CNF template.

Further insights into the structural changes after doping of P element could be acquired from the Raman spectra and XPS analysis. As shown by the Raman spectra in Fig. 3B, the $NiCo_2S_4$@CNT/CNF hybrid displays four peaks at 241.7 $cm^{-1}$,

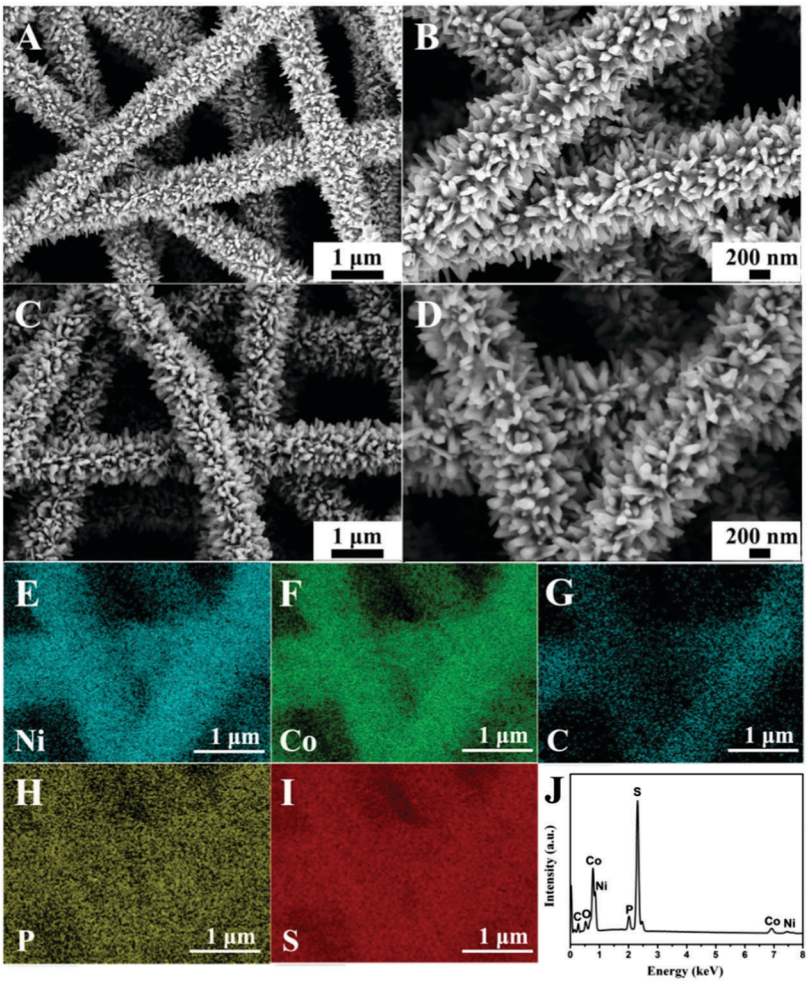


Fig. 2 FESEM images of (A and B) the $NiCo_2S_4$@CNT/CNF hybrid and (C and D) the P-$NiCo_2S_4$@CNT/CNF hybrid, (E–I) EDS mapping images of the P-$NiCo_2S_4$@CNT/CNF hybrid, and (J) EDS spectrum of the P-$NiCo_2S_4$@CNT/CNF hybrid.

384.9 $cm^{-1}$, 305.7 $cm^{-1}$, and 352.9 $cm^{-1}$, which are the characteristic $E_g$, $A_{1g}$, and two $T_{2g}$ vibration modes of $NiCo_2S_4$.[7] Besides, some additional vibration modes in the range of 400 $cm^{-1}$–800 $cm^{-1}$ can be obviously observed, which can be well indexed to the Raman features of $NiCo_2O_4$,[23] as the surface of transitional metal sulfides can be easily oxidized once exposed to air.[24,25] After the phosphidation reaction, the peaks in the range of 400 $cm^{-1}$–800 $cm^{-1}$ disappeared for the P-$NiCo_2S_4$@CNT/CNF hybrid, which is due to the fact that the released $PH_3$ during phosphidation can reduce the superficial oxide impurities into the P-doped $NiCo_2S_4$ hybrid.

As shown in Fig. 3C, the Co 2p spectrum displays low energy bands (Co $2p_{3/2}$) and high energy bands (Co $2p_{1/2}$).[26] Specifically, the binding energies centered at 779.40 eV and 794.60 eV of the Co 2p peaks correspond to the $Co^{3+}$ state while those at 783.70 eV and 799.20 eV are characteristic of the $Co^{2+}$ state. Similarly, for the Ni 2p spectrum, the peaks located at 854.20 eV and 871.50 eV can be respectively assigned to Ni $2p_{3/2}$ and Ni $2p_{1/2}$ spin orbits of the $Ni^{2+}$ state, and those situated at 857.90 eV and 876.20 eV are associated with the $Ni^{3+}$ state.[21,27] Besides, it is interesting to notice that the relative peak intensities of the $Ni^{2+}$ state and $Co^{3+}$ state for the P-$NiCo_2S_4$@CNT/CNF hybrid are higher than those for the $NiCo_2S_4$@CNT/CNF hybrid, further confirming that $NiCo_2S_4$ in the P-$NiCo_2S_4$@CNT/CNF hybrid shows much higher crystalline purity. For the S 2p spectrum, the S 2p spectrum has been fitted with spin–orbit doublet separation of 1.18 eV and an area ratio of 2 : 1. The peaks located at 161.00 eV and 162.18 eV, respectively, correspond to S $2p_{3/2}$ and S $2p_{1/2}$ orbits of divalent sulfide ions ($S^{2-}$). However, no obvious peak can be fitted for the $S_2^{2-}$ $2p_{3/2}$ and $S_2^{2-}$ $2p_{1/2}$ at 163.20 eV and 164.38 eV, indicating that no S-rich structure exists in the P-$NiCo_2S_4$@CNT/CNF and $NiCo_2S_4$@CNT/CNF hybrids. Moreover, an extra peak at 168.30 eV induced by sulfur oxide can be obviously observed for the S 2p spectrum of the $NiCo_2S_4$@CNT/CNF hybrid, which is not observed for the P-$NiCo_2S_4$@CNT/CNF hybrid. This further confirms that phosphidation reaction helps to remove some sulfur oxides triggered by surface air oxidization, which is consistent with the Raman results.[28] With regard to the P 2p spectrum of the P-$NiCo_2S_4$@CNT/CNF hybrid, two peaks with binding energies of 128.90 eV and 129.90 eV are, respectively, assigned to P $2p_{3/2}$ and P $2p_{1/2}$, along with a characteristic peak attributed to phosphate-like P at 133.45 eV.[19,29,30] As a result, although

 

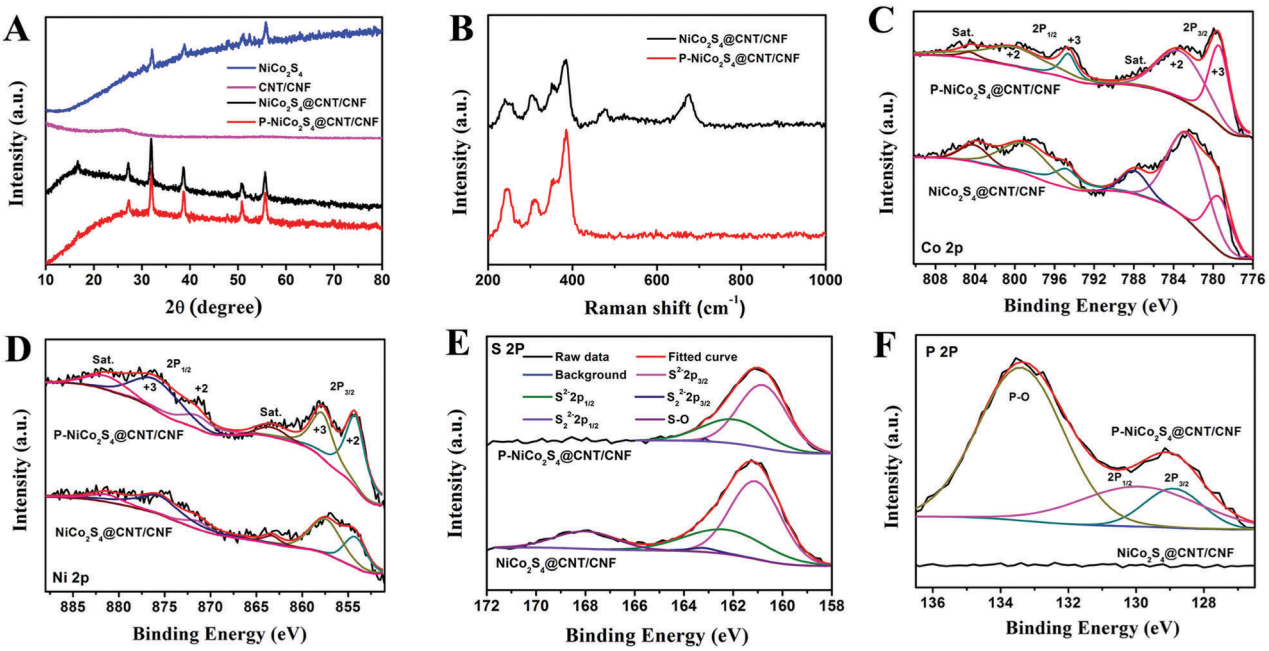


Fig. 3 (A) XRD patterns of different products. (B) Raman spectra of the $NiCo_2S_4$@CNT/CNF and P-$NiCo_2S_4$@CNT/CNF hybrids. (C–F) XPS spectra of the $NiCo_2S_4$@CNT/CNF and P-$NiCo_2S_4$@CNT/CNF hybrids: high-resolution (C) Co 2p, (D) Ni 2p, (E) S 2p, and (F) P 2p spectra.

phosphidation reaction removes the S–O peak, it induces a P–O peak of phosphate at the same time. However, some studies report that metal phosphates are electrocatalytically active to a certain degree.[31,32] By contrast, the $NiCo_2S_4$@CNT/CNF hybrid does not show any significant peaks in the corresponding range of binding energy. All the above results strongly prove the successful doping of P element into the $NiCo_2S_4$@CNT/CNF hybrid.

### 3.2. HER electrocatalytic activity of the P-$NiCo_2S_4$@CNT/CNF hybrid

The electrocatalytic performance of the HER catalysts was measured with a standard three-electrode setup in 0.5 M $H_2SO_4$ electrolyte. From the polarization curves in Fig. 4A, it is shown that the onset overpotential ($\eta$) is only 27 mV for the P-$NiCo_2S_4$@CNT/CNF hybrid, which is the lowest among all the as-prepared products. Moreover, the drive current density ($j$) of 10 mA $cm^{-2}$, a characteristic value for solar fuel conversion, can be achieved at a small overpotential of 74 mV for the P-$NiCo_2S_4$@CNT/CNF hybrid, compared with 126 mV for the P-$NiCo_2S_4$@CNF hybrid, 164 mV for the $NiCo_2S_4$@CNT/CNF hybrid and 278 mV for $NiCo_2S_4$, respectively. As is well known, an excellent electrocatalyst is desirable to drive significant current densities with low overpotentials. Therefore, the P-$NiCo_2S_4$@CNT/CNF hybrid exhibits the optimal HER activities among all the prepared products, demonstrating that P doping, CNT reinforcement, and template-confined growth can help enhance the electrocatalytic performance of catalysts. Furthermore, it is worth noting that for the same current density ($j$ = 10 mA $cm^{-2}$), the difference of the required overpotential between the $NiCo_2S_4$@CNT/CNF and P-$NiCo_2S_4$@CNT/CNF electrocatalysts is up to nearly 100 mV, highlighting the significant impacts induced by P-doping. The electrochemical double-layer capacitance ($C_{dl}$), which is linearly proportional to the electrocatalytically active surface area, was investigated to explain the differences in HER performance of various catalysts. As shown in Fig. 4B and Fig. S4 (ESI†), the $C_{dl}$ of the P-$NiCo_2S_4$@CNT/CNF hybrid is tested to be 33.8 mF $cm^{-2}$, which is far beyond that of other counterparts, indicating the existence of more electrocatalytic sites. The unique nanostructure of the P-$NiCo_2S_4$@CNT/CNF hybrid makes great contributions to its increased HER active sites. First, the electronic structure of catalytically active $NiCo_2S_4$ can be improved with P doping, thus tuning the hydrogen adsorption free energy ($\Delta G_H$) closer to thermoneutral. Second, CNTs increase the electrical conductivity of the CNF template, which facilitates the electron transport between the 3D template and $NiCo_2S_4$ nanocrystals. Last but not least, with the CNT/CNF network, $NiCo_2S_4$ is confined to grow into perpendicularly oriented nanocrystals instead of agglomerates, thus constructing a hierarchical structure with exposed active sites on a nanoscale size. These synergistic effects lead to the increase in the number of catalytic sites of the P-$NiCo_2S_4$@CNT/CNF hybrid, making contributions to its distinctive HER performance.

In addition, Tafel plots are derived by plotting overpotential ($\eta$) against log current ($\log j$), and the kinetic parameters can be calculated (Fig. 4C). The linear parts of the Tafel plots reveal that Tafel slopes of all prepared electrocatalysts are in the range of 60 mV $decade^{-1}$–75 mV $decade^{-1}$, suggesting that the HER activities proceed *via* a fast Volmer reaction, followed by a rate-limiting Heyrovsky step. The exchange current density, $j_0$, which is obtained from the Tafel curves with the extrapolation method, can reflect the inherent HER activity of the catalyst. As shown in Fig. S5 and Table S2 (ESI†), the exchange current density ($j_0$) for the P-$NiCo_2S_4$@CNT/CNF hybrid is 0.79 mA $cm^{-2}$, which is 4–20 times larger than that of the other hybrids, presenting its intrinsic outstanding activity for HER catalysis.

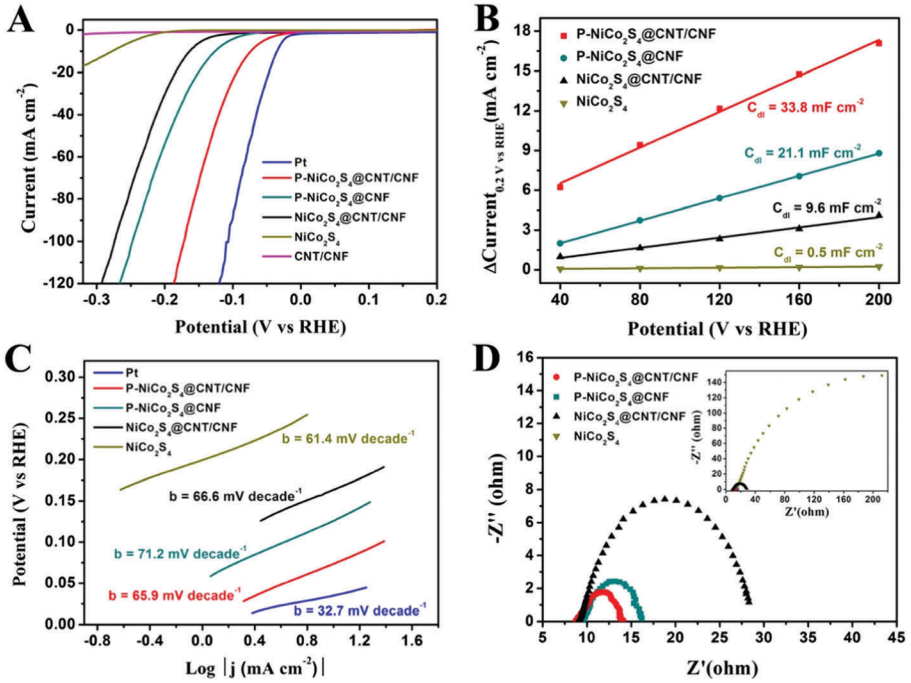


Fig. 4 (A) LSV polarization curves for the CNT/CNF, $NiCo_2S_4$, and $NiCo_2S_4$@CNT/CNF and P-$NiCo_2S_4$@CNT/CNF hybrid modified GCE in $N_2$-purged 0.5 M $H_2SO_4$ solution. (B) Plot showing the extraction of the double layer capacitance ($C_{dl}$) for the different hybrids at 0.2 V *versus* RHE. (C) Tafel plots for the different hybrid modified GCEs. (D) Nyquist plots of the different hybrids at overpotential of 0.17 V *versus* RHE.

The large $j_0$ can be attributed to the P-doping induced change in electronic structure of $NiCo_2S_4$, which further lowers the kinetic energy barrier during the hydrogen formation process, thus generating a remarkable improvement in the inherent catalytic performance. It is worth mentioning that the HER activities of the P-$NiCo_2S_4$@CNT/CNF hybrid exceed most reported studies (Table 1), further illustrating its ultra-high catalytic ability. The electrochemical impedance spectroscopy (EIS) measurement was also explored under the HER process (Fig. 4D). Nyquist plots reveal that the P-$NiCo_2S_4$@CNT/CNF hybrid shows the smallest charge transfer resistance ($R_{ct}$) of 4.7 Ω among all the products, reflecting its rapid electron transfer compared with its counterparts.

The stability of the P-$NiCo_2S_4$@CNT/CNF catalyst was measured through performing continuous HER activities at a constant overpotential of 125 mV. As shown in Fig. 5A and B, there occurs only a slight fluctuation in such a large current density (around 40 mA cm$^{-2}$) for 10 h, along with no distinct changes in its polarization curves measured after cycling. Furthermore, the charge transfer resistance ($R_{ct}$) only slightly increases from 7.9 Ω to 9.1 Ω (Fig. 5C) after cycling for 10 h. All the results indicate the excellent HER stability of the P-$NiCo_2S_4$@CNT/CNF hybrid catalyst, which can be attributed to its robust morphology that is retained well during the violent hydrogen evolution reaction (Fig. 5D).

Table 1 Comparison of the HER activity of the P-$NiCo_2S_4$@CNT/CNF hybrid to the reported electrocatalysts

| Sample | $\eta_0$ (mV) | $\eta_{10}$ (mV) | Ref. |
|---|---|---|---|
| $Mn_{0.05}Co_{0.95}Se_2$ | 174 | 195 | 33 |
| $NiP_{1.93}Se_{0.07}$/carbon paper | | 84 | 18 |
| Co-doped $MoS_2$/carbon black | 90 | 135 | 34 |
| Hollow $Zn_{0.30}Co_{2.70}S_4$ | 35 | 80 | 10 |
| $MoS_2$/$CoS_2$/carbon cloth | | 87 | 35 |
| P doped $MoO_2$ on Mo foil | 80 | 135 | 19 |
| $Co_xW_{(1-x)}S_2$ | | 121 | 36 |
| SnS/N-doped graphene | 59 | 125 | 37 |
| P-$NiCo_2S_4$@CNT/CNF | 27 | 74 | This work |

$\eta_0$: onset overpotential; $\eta_{10}$: overpotential ($\eta$) for current density ($j$) of 10.0 mA cm$^{-2}$.

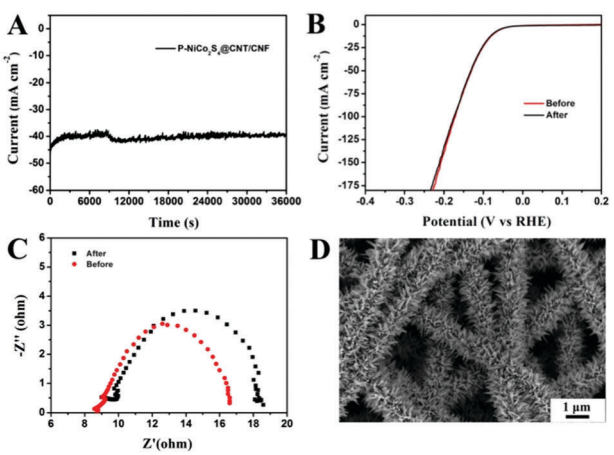


Fig. 5 (A) Time dependence of the current density for the P-$NiCo_2S_4$@CNT/CNF hybrid modified GCE recorded at −0.17 V *versus* RHE. (B) Comparison of LSV polarization curves for the P-$NiCo_2S_4$@CNT/CNF hybrids before and after the cycling test. (C) Comparison of Nyquist plots for the P-$NiCo_2S_4$@CNT/CNF hybrids before and after the cycling test. (D) FESEM image of the P-$NiCo_2S_4$@CNT/CNF hybrids after the cycling test.

 

# 4. Conclusions

In summary, we have successfully prepared P-$NiCo_2S_4$@CNT/CNF hybrid catalysts by combining electrospinning, a hydrothermal method, and phosphidation reaction. The involvement of CNTs increases the electrical conductivity of the CNF template, which provides fast electron transfer to the attached $NiCo_2S_4$ nanocrystals. Templated by the CNT/CNF network, $NiCo_2S_4$ is confined to grow into perpendicularly oriented nanocrystals instead of agglomerates, thus constructing a hierarchical structure with increased electrocatalytically active sites. The phosphidation reaction realizes the doping of P into the hybrid, thereby decreasing the kinetic energy barrier. Consequently, the P-$NiCo_2S_4$@CNT/CNF hybrid exhibits outstanding HER activities with a low onset overpotential ($\eta$) of 27 mV, a large cathodic current of 10 mA $cm^{-2}$ at $\eta$ of only 74 mV, an impressive exchange current density of 0.79 mA $cm^{-2}$ and excellent long-term durability in acid solution, which are superior to most reported noble-metal-free electrocatalysts and comparable to that of Pt. The strategy of heteroatom doping into electroactive materials and conductivity enhancement on templates, provides an efficient method to fabricate highly active electrocatalysts for energy conversion.

# Acknowledgements

The authors are grateful for the financial support from the National Natural Science Foundation of China (51433001, 51373037), and the Program of Shanghai Academic Research Leader (17XD1400100).

# Notes and references

1 A. G. Tamirat, J. Rick, A. A. Dubale, W. N. Su and B. J. Hwang, *Nanoscale Horiz.*, 2016, **1**, 243–267.
2 A. Vasileff, S. Chen and S. Z. Qiao, *Nanoscale Horiz.*, 2016, **1**, 41–44.
3 F. L. Lai, D. Y. Yong, X. L. Ning, B. C. Pan, Y. E. Miao and T. X. Liu, *Small*, 2016, 1602866.
4 W. Gao, Y. Q. Shi, Y. F. Zhang, L. Z. Zuo, H. Y. Lu, Y. P. Huang, W. Fan and T. X. Liu, *ACS Sustainable Chem. Eng.*, 2016, **4**, 6313–6321.
5 Y. Pan, Y. Lin, Y. J. Chen, Y. Q. Liu and C. G. Liu, *J. Mater. Chem. A*, 2016, **4**, 4745–4754.
6 K. Ojha, S. Saha, B. Kumar, K. S. Hazra and A. K. Ganguli, *ChemCatChem*, 2016, **8**, 1218–1225.
7 C. Xia, P. Li, A. N. Gandi, U. Schwingenschlögl and H. N. Alshareef, *Chem. Mater.*, 2015, **27**, 6482–6485.
8 W. B. Fu, C. H. Zhao, W. H. Han, Y. Liu, H. Zhao, Y. F. Ma and E. Q. Xie, *J. Mater. Chem. A*, 2015, **3**, 10492–10497.
9 C. Xia and H. N. Alshareef, *Chem. Mater.*, 2015, **27**, 4661–4668.
10 Z. F. Huang, J. J. Song, K. Li, M. Tahir, Y. T. Wang, L. Pan, L. Wang, X. W. Zhang and J. J. Zou, *J. Am. Chem. Soc.*, 2016, **138**, 1359–1365.
11 S. J. Peng, L. L. Li, J. Kong Yoong Lee, L. L. Tian, M. Srinivasan, S. Adams and S. Ramakrishna, *Nano Energy*, 2016, **22**, 361–395.
12 Z. X. Dong, S. J. Kennedy and Y. Q. Wu, *J. Power Sources*, 2011, **196**, 4886–4904.
13 Z. Y. Xiong, X. Y. Kong, Z. X. Guo and J. Yu, *Chin. J. Polym. Sci.*, 2015, **33**, 1234–1244.
14 F. L. Lai, Y. E. Miao, Y. P. Huang, T. S. Chung and T. X. Liu, *J. Phys. Chem. C*, 2015, **119**, 13442–13450.
15 J. K. Nørskov, T. Bligaard, A. Logadottir, J. R. Kitchin, J. G. Chen, S. Pandelov and U. Stimming, *J. Electrochem. Soc.*, 2005, **152**, J23–J26.
16 Q. F. Gong, L. Cheng, C. H. Liu, M. Zhang, Q. L. Feng, H. L. Ye, M. Zeng, L. M. Xie, Z. Liu and Y. G. Li, *ACS Catal.*, 2015, **5**, 2213–2219.
17 K. Xu, F. M. Wang, Z. X. Wang, X. Y. Zhan, Q. S. Wang, Z. Z. Cheng, M. Safdar and J. He, *ACS Nano*, 2014, **8**, 8468–8476.
18 J. Q. Zhuo, M. Cabán-Acevedo, H. F. Liang, L. Samad, Q. Ding, Y. P. Fu, M. X. Li and S. Jin, *ACS Catal.*, 2015, **5**, 6355–6361.
19 X. Xie, R. J. Yu, N. Xue, A. B. Yousaf, H. Du, K. Liang, N. Jiang and A. W. Xu, *J. Mater. Chem. A*, 2016, **4**, 1647–1652.
20 J. Yang, M. Z. Ma, C. C. Sun, Y. F. Zhang, W. Huang and X. C. Dong, *J. Mater. Chem. A*, 2015, **3**, 1258–1264.
21 J. G. Wang, D. D. Jin, R. Zhou, C. Shen, K. Y. Xie and B. Q. Wei, *J. Power Sources*, 2016, **306**, 100–106.
22 D. Y. Wang, M. Gong, H. L. Chou, C. J. Pan, H. A. Chen, Y. P. Wu, M. C. Lin, M. Y. Guan, J. Yang, C. W. Chen, Y. L. Wang, B. J. Hwang, C. C. Chen and H. J. Dai, *J. Am. Chem. Soc.*, 2015, **137**, 1587–1592.
23 C. F. Windisch Jr. and G. J. Exarhos, *J. Appl. Phys.*, 2002, **92**, 5572–5574.
24 L. S. Zhang, Y. P. Huang, Y. F. Zhang, H. H. Gu, W. Fan and T. X. Liu, *Adv. Mater. Interfaces*, 2016, **3**, 1500467.
25 H. H. Gu, Y. P. Huang, L. Z. Zuo, W. Fan and T. X. Liu, *Electrochim. Acta*, 2016, **219**, 604–613.
26 J. W. Xiao, L. Wan, S. H. Yang, F. Xiao and S. Wang, *Nano Lett.*, 2014, **14**, 831–838.
27 Z. C. Li, Y. Qu, M. G. Wang, Y. M. Hu, J. Han, L. Fan and R. Guo, *Colloid Polym. Sci.*, 2016, **294**, 1325–1332.
28 D. L. Legrand, H. W. Nesbitt and G. M. Bancroft, *Am. Mineral.*, 1998, **83**, 1256–1265.
29 G. Y. Xu, B. Ding, J. Pan, J. P. Han, P. Nie, Y. Zhu, Q. Sheng and H. Dou, *J. Mater. Chem. A*, 2015, **3**, 23268–23273.
30 W. Liu, E. Y. Hu, H. Jiang, Y. J. Xiang, Z. Weng, M. Li, Q. Fan, X. Q. Yu, E. I. Altman and H. L. Wang, *Nat. Commun.*, 2016, **7**, 10771.
31 J. H. Xing, H. Li, M. C. C. Mark, S. M. Geyer and K. Y. S. Ng, *J. Mater. Chem. A*, 2016, **4**, 13866–13873.
32 Z. X. Cai, W. Xu, F. M. Li, Q. H. Yao and X. Chen, *ACS Sustainable Chem. Eng.*, 2017, **5**, 571–579.
33 Y. W. Liu, X. M. Hua, C. Xiao, T. F. Zhou, P. C. Huang, Z. P. Guo, B. C. Pan and Y. Xie, *J. Am. Chem. Soc.*, 2016, **138**, 5087–5092.
34 X. P. Dai, K. L. Du, Z. Z. Li, M. Z. Liu, Y. D. Ma, H. Sun, X. Zhang and Y. Yang, *ACS Appl. Mater. Interfaces*, 2015, **7**, 27242–27253.
35 J. L. Huang, D. M. Hou, Y. C. Zhou, W. J. Zhou, G. Q. Li, Z. H. Tang, L. G. Li and S. W. Chen, *J. Mater. Chem. A*, 2015, **3**, 22886–22891.
36 T. A. Shifa, F. M. Wang, K. L. Liu, K. Xu, Z. X. Wang, X. Y. Zhan, C. Jiang and J. He, *Small*, 2016, **12**, 3802–3809.
37 S. S. Shinde, A. Sami, D. Kim and J. Lee, *Chem. Commun.*, 2015, **51**, 15716–15719.